

## Supplementary Materials for

### **A novel artificial condensed matter lattice and a new platform for one-dimensional topological phases**

Ilya Belopolski, Su-Yang Xu, Nikesh Koirala, Chang Liu, Guang Bian, Vladimir N. Strocov, Guoqing Chang, Madhab Neupane, Nasser Alidoust, Daniel Sanchez, Hao Zheng, Matthew Brahlek, Victor Rogalev, Timur Kim, Nicholas C. Plumb, Chaoyu Chen, François Bertran, Patrick Le Fèvre, Amina Taleb-Ibrahimi, Maria-Carmen Asensio, Ming Shi, Hsin Lin, Moritz Hoesch, Seongshik Oh, M. Zahid Hasan

Published 24 March 2017, *Sci. Adv.* **3**, e1501692 (2017)

DOI: 10.1126/sciadv.1501692

#### **This PDF file includes:**

- Estimate of indium diffusion in the heterostructure
- Observation of a topological phase transition in numerics
- Fine dependence on indium doping
- Comparison with a single thin film of  $\text{Bi}_2\text{Se}_3$
- Detailed analysis of bulk quantum well states
- fig. S1. Characterization of In diffusion in the heterostructures.
- fig. S2. Topological phase transition in numerics.
- fig. S3. Change in Fermi level with In doping.
- fig. S4. Dimerized-limit heterostructure and a single thin film of  $\text{Bi}_2\text{Se}_3$ .
- fig. S5. Bulk quantum well states of 4QL/2QL 15% and 4QL/1QL 20%.
- Reference (25)

## Estimate of indium diffusion in the heterostructure

It is important to check that diffusion of In within the sample does not remove the layered  $\text{Bi}_2\text{Se}_3/\text{In}_x\text{Bi}_{2-x}\text{Se}_3$  pattern of the heterostructure. In this section, we characterize In diffusion in our heterostructures. In subsequent sections, we also provide a number of checks in ARPES which confirm indirectly that the heterostructure consists of clean interfaces. We show a high-angle annular dark-field scanning transmission electron microscopy (HAADF-STEM) image, fig. S1B, of a thin film with alternating layers of  $\text{Bi}_2\text{Se}_3$  and  $\text{In}_2\text{Se}_3$  of different thicknesses [11]. Sharp interfaces between the  $\text{In}_2\text{Se}_3$  and  $\text{Bi}_2\text{Se}_3$  indicate no substantial diffusion between the layers. We also measure a heterostructure consisting of a single  $\text{Bi}_2\text{Se}_3/\text{In}_x\text{Bi}_{2-x}\text{Se}_3$  unit cell, with the  $\text{Bi}_2\text{Se}_3$  on top, see fig. S1C. We use scanning tunneling microscopy (STM) to count the number of In atoms that diffuse to the top QL of  $\text{Bi}_2\text{Se}_3$ , see Ref. 24 for details of the STM measurement. For both 30QL/20QL 50% and 5QL/20QL 50% films grown at  $275^\circ\text{C}$ , we find  $\sim 0.2\%$  In diffusion to the top QL of  $\text{Bi}_2\text{Se}_3$  [25]. This indicates that there is minimal In diffusion at  $x = 50\%$  and also that there is no significant variation of In diffusion with the thickness of the  $\text{Bi}_2\text{Se}_3$  layer. To gain insight into the effect of growth temperature and doping  $x$ , we further studied 3QL/20QL 50% grown at  $300^\circ\text{C}$  and 30QL/20QL 100% grown at  $275^\circ\text{C}$ . We found  $\sim 2\%$  and  $\sim 1.3\%$  In diffusion to the top QL of the  $\text{Bi}_2\text{Se}_3$  layer, respectively (data not shown). Clearly (and perhaps not unexpectedly) In diffusion is suppressed with lower growth temperature and lower  $x$ . Since the heterostructures studied here are grown at  $265^\circ\text{C}$  with  $x \leq 25\%$ , In diffusion should be considerably suppressed even compared to the  $\sim 0.2\%$  diffusion observed for 30QL/20QL 50% and 5QL/20QL 50% grown at  $275^\circ\text{C}$ . We note that the topological phase transition for  $\text{In}_x\text{Bi}_{2-x}\text{Se}_3$  occurs at  $x \sim 4\%$ , so we can conclude that In diffusion in our heterostructures is easily low enough to ensure that the  $\text{Bi}_2\text{Se}_3$  and  $\text{In}_x\text{Bi}_{2-x}\text{Se}_3$  layers remain topological and trivial, respectively. Lastly, we suggest that a characterization by X-ray diffraction could supply other useful insights relating to the quality of interfaces in our samples, but we do not attempt this measurement here. Our direct characterization of In diffusion in our samples shows quite conclusively that In diffusion does not remove the layered pattern of the heterostructure.

## Observation of a topological phase transition in numerics.

We perform a tight-binding calculation of the band structure of our topological insulator heterostructure. We consider only hopping between Se  $p$  orbitals within the Se planes and between the Se planes of  $\text{Bi}_2\text{Se}_3$ , with hopping  $t$  within the topological layer,  $t'$  within the trivial layer and  $t''$  at the interface between layers. By tuning the hopping parameters, we observe a band inversion between the two superlattice bands, associated with a topological phase transition between a topological insulator and a trivial insulator, shown in fig. S2. We also plot the wavefunction of a specific state in real space, showing that the state is localized only at the heterostructure interfaces.

## Fine dependence on indium doping

We provide an additional, independent check that there is no In diffusion at least near the top of our heterostructure. We present  $E$ - $k$  cuts through  $\bar{\Gamma}$  of 4QL/1QL heterostructures with In doping 5%, 8%, 10%, 15%, 20% and 25% at an incident photon energy of  $h\nu = 18$  eV, shown in fig. S3.

We consider the separation between the inner bulk conduction quantum well state and the Dirac point and we observe that this energy difference is  $\sim 0.2$  eV independent of the In doping. We make similar observations about the other bulk conduction quantum well state as well as the bulk valence quantum well states. We note that bulk  $\text{Bi}_2\text{Se}_3$  is very sensitive to In doping, with a topological phase transition at only  $\sim 4\%$  In. However, the trivial In doping in these heterostructures changes by 20% without any gap closing in the quantum well states of the top layer. This shows that In does not diffuse into the topmost topological layer from the topmost trivial layer. At the same time, we observe that the Fermi level rises with increasing In doping. This rise in the Fermi level is again inconsistent with In diffusion into the  $\text{Bi}_2\text{Se}_3$  layer because the bulk conduction band recedes above the Fermi level with increasing  $x$  in  $\text{In}_x\text{Bi}_{2-x}\text{Se}_3$  [11]. We suggest that the rise in the Fermi level with In doping may result from the large band gap of the topologically trivial layers. Specifically, the topological and trivial layers have different carrier density, leading to a band-bending effect that may correspond to an effective  $n$  doping on the top  $\text{Bi}_2\text{Se}_3$  layer. Regardless of the mechanism of  $n$  doping, we note that this systematic shift of the Fermi level with In doping confirms that the In concentration indeed increases in the trivial layers. The dependence of the bulk gap and Fermi level on In doping shows that the heterostructure consists of high-quality interfaces.

### **Comparison with a single thin film of $\text{Bi}_2\text{Se}_3$ .**

We present yet another, independent check that the heterostructure is well-defined by considering dimerized-limit heterostructures. We repeat the  $E$ - $k$  cuts through  $\bar{\Gamma}$  of 3QL/3QL 20%, 4QL/4QL 20% and 10QL/10QL 20%, discussed in the main text, and we show earlier results on single thin films of  $\text{Bi}_2\text{Se}_3$ , from [16]. We see that the size of the gap in the topological surface states is  $\sim 0.2$  eV for a single 3QL film of  $\text{Bi}_2\text{Se}_3$ , but  $\sim 0.15$  eV for 3QL/3QL 20%, as shown in fig. S4. Further, the gap is  $\sim 0.1$  eV for both 4QL/4QL 20% and a single thin film 4QL thick. Lastly, the gap for a single thin film vanishes above 7QL, and we observe a gapless surface state in 10QL/10QL 20%. If there were In diffusion from the topmost trivial layer to the topmost topological layer, then the effective thickness of the topological layer should decrease, causing the surface state gap to increase. Since the gap in the heterostructure is no larger than the gap in the corresponding single thin film, there is no In diffusion into the topmost topological layer. Incidentally, the  $\sim 0.15$  eV gap in 3QL/3QL 20% therefore shows an emergent superlattice band structure away from the dimerized limit, with small but observable hopping across the trivial layer. Our comparison of topological insulator heterostructures with single thin films of  $\text{Bi}_2\text{Se}_3$  again shows that the heterostructure consists of high-quality interfaces.

### **Detailed analysis of bulk quantum well states**

To clearly demonstrate the pair of bulk conduction quantum well states in 4QL/2QL 15% and 4QL/1QL 20%, we present additional analysis of the spectra that were shown in Fig. 2G, H of the main text. In fig. S5A, we show a second-derivative map for 4QL/2QL 15%, to complement the second-derivative map shown for 4QL/1QL 20% in main text Fig. 3B. We also show the raw data in several color scales, to make the features more visible. We clearly observe two bulk conduction quantum well states in both spectra, as well as a gapless topological surface state and bulk valence quantum well states.

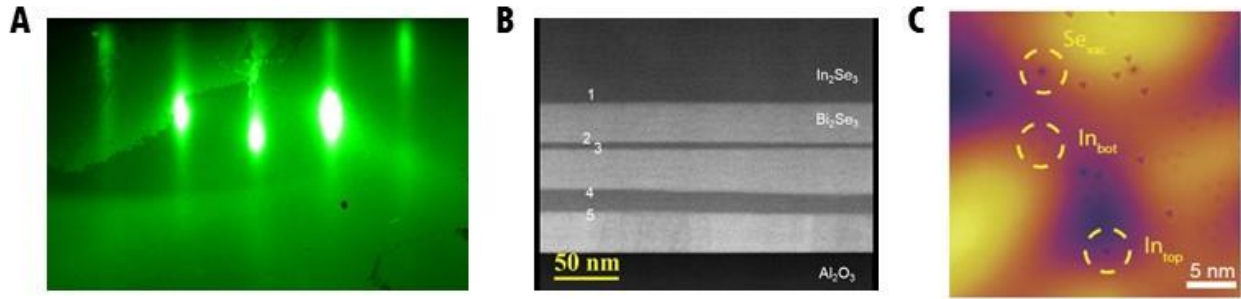


**fig. S1. Characterization of In diffusion in the heterostructures.** (A) Reflection high-energy electron diffraction (RHEED) image showing an atomically flat single crystalline growth, as indicated by the sharp streaks and Kikuchi lines. This confirms the high quality of our heterostructures. (B) High-angle annular dark-field scanning transmission electron microscopy (HAADF-STEM) image of a  $\text{Bi}_2\text{Se}_3/\text{In}_2\text{Se}_3$  heterostructure, showing sharp interfaces between the layers. The sample has layer pattern 100  $\text{In}_2\text{Se}_3/30 \text{ Bi}_2\text{Se}_3/5 \text{ In}_2\text{Se}_3/30 \text{ Bi}_2\text{Se}_3/20 \text{ In}_2\text{Se}_3/30 \text{ Bi}_2\text{Se}_3$ , demonstrating at the same time the sharp interfaces in our heterostructure as well as our ability to precisely control the layer thickness in MBE. (C) Indium atoms observed on  $\text{Bi}_2\text{Se}_3$  by scanning tunneling microscopy (STM) in a 5QL/20QL 50% heterostructure with one superlattice unit cell.  $\text{In}_{\text{top}}$  and  $\text{In}_{\text{bot}}$  represent In atoms diffused to the top and bottom Bi layer within the topmost QL of  $\text{Bi}_2\text{Se}_3$ , while  $\text{Se}_{\text{vac}}$  represent Se vacancies. (Reprinted with permission from Ref. (25), © 2015 American Chemical Society).

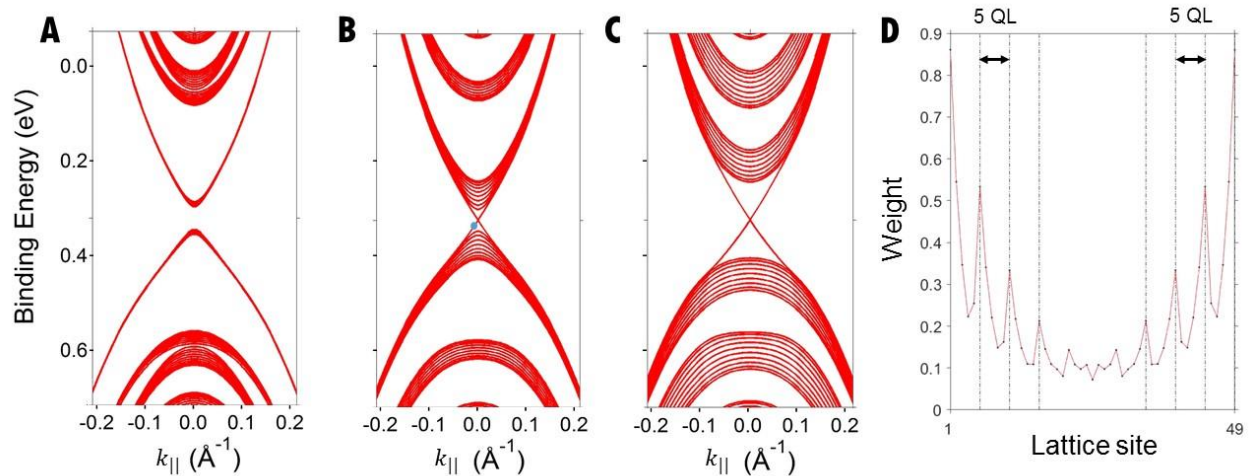


**fig. S2. Topological phase transition in numerics.** Dispersion of a tight-binding model taking into account hopping between Se  $p$  orbitals in a topological insulator heterostructure. Changing the hopping amplitudes shows (A) a trivial insulator with gapped superlattice band, (B) a phase near the critical point, with a superlattice band at the critical point and (C) a topological insulator with a gapped superlattice band and gapless surface state. (D) Wavefunction of a superlattice state, showing that the state is spatially localized at the interfaces of the heterostructure. The plotted state is marked by the blue circle in (B). Note that in this model we do not *a priori* assume any topological surface or interface states.

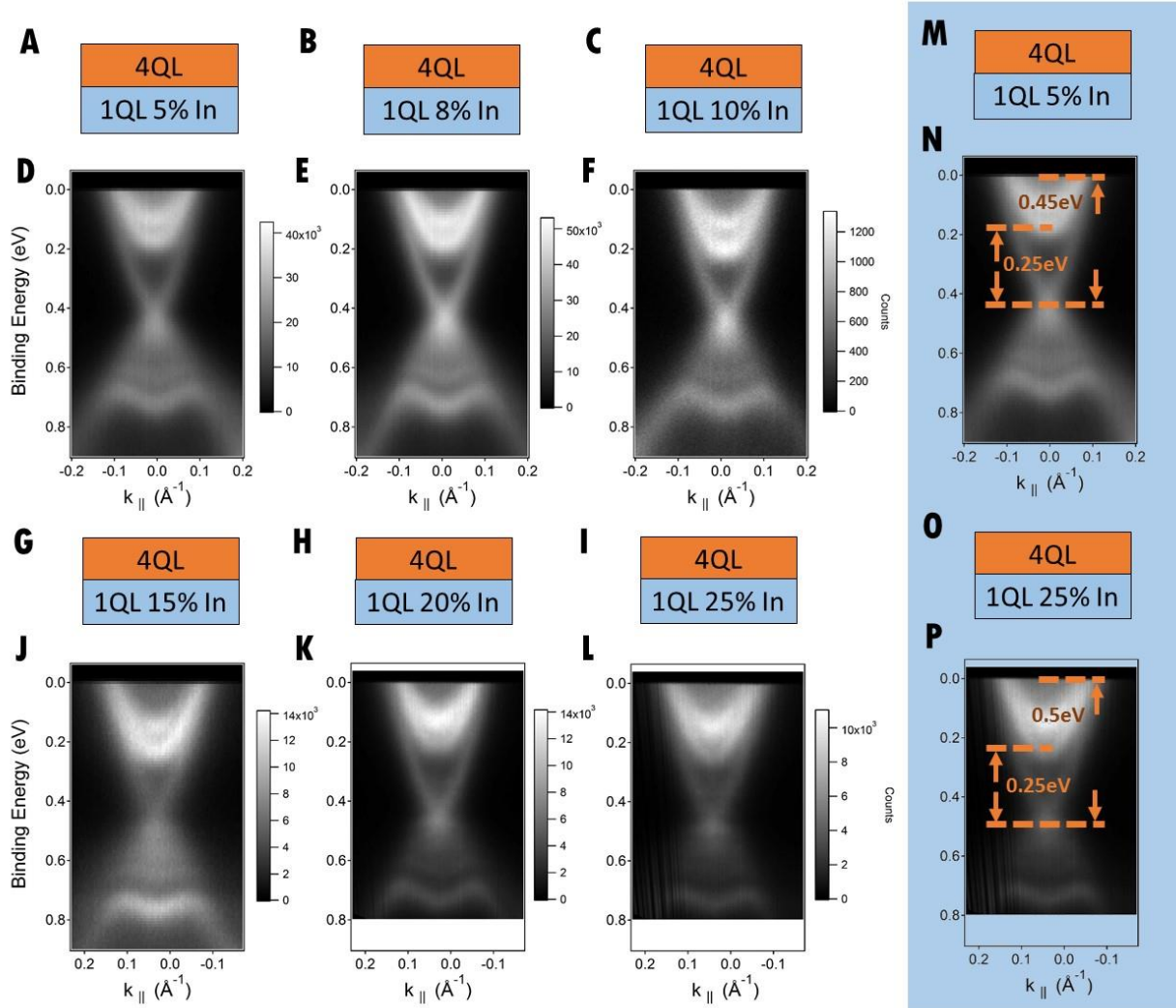


**fig. S3. Change in Fermi level with In doping.** Systematic study of heterostructures with compositions shown in (A–C) and (G–I). All samples have 4QL topological layers and 1QL trivial layers, but have varying In doping in the trivial layer. (D–F, J–L) ARPES spectra, showing an  $E$ - $k$  cut through  $\bar{\Gamma}$ . We see that the bulk valence and conduction band quantum well states do not change as a function of In doping. In particular, the bulk band gap does not decrease despite a 20% increase in In doping in the adjacent trivial layer, showing that there is no observable In diffusion to the topmost topological layer. At the same time, the Fermi level rises further into the bulk conduction band. This  $n$  doping clearly increases with In doping and we speculate that it is due to the large band gap of the trivial layer under large In doping. Blue panel: we show again the first and last composition in this series, with 5% In (M) and 25% In (O). (N, P) The distance between the conduction band minimum and the Dirac point is  $\sim 0.25$  eV for both compositions, but the Fermi level moves upward, so the Dirac point is  $\sim 0.45$  eV below the Fermi level for 5% In and  $\sim 0.5$  eV below the Fermi level for 25% In. We see that while the bulk band gap of the topmost topological layer does not begin to close, the In doping in the trivial layer is different in the different samples. This shows that the heterostructure consists of sharp interfaces.

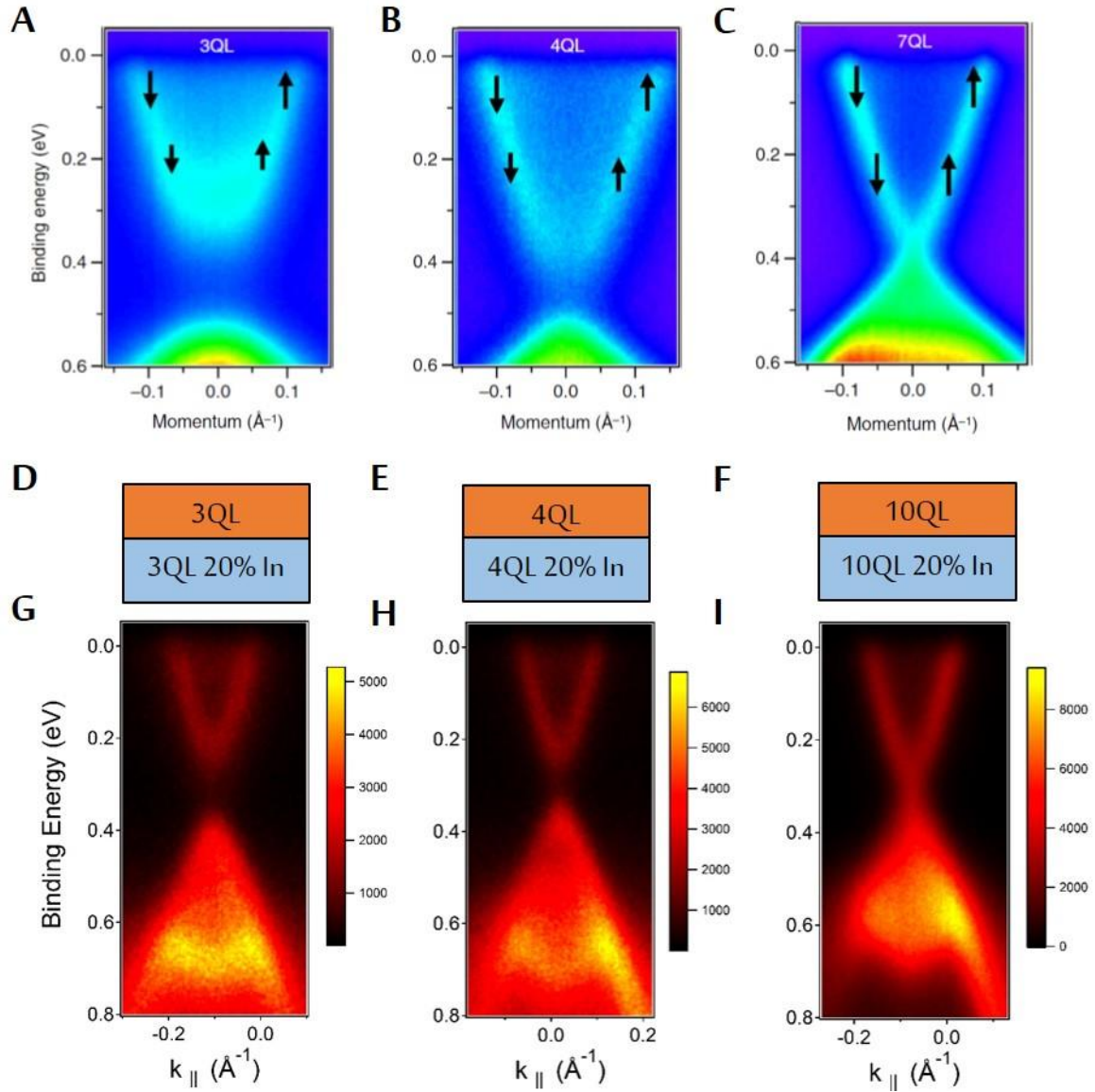


**fig. S4. Dimerized-limit heterostructure and a single thin film of Bi<sub>2</sub>Se<sub>3</sub>.** (A–C) Gapped topological surface states in a single thin film of Bi<sub>2</sub>Se<sub>3</sub>, of thickness 3QL, 4QL and 7QL, respectively, adapted from [16]. (D–F) Unit cells of heterostructures 3QL/3QL 20%, 4QL/4QL 20% and 10QL/10QL 20%. (G–I) ARPES spectra, showing an  $E$ - $k$  cut through  $\bar{\Gamma}$ . The band gap is  $\sim 0.2$  eV in the single 3QL thin film, but  $\sim 0.15$  eV in 3QL/3QL 20%. The band gap is  $\sim 0.1$  eV in both the single 4QL thin film and 4QL/4QL 20%. The surface state is gapless for the single 7QL thin film and 10QL/10QL 20%. The difference in the band gap at 3QL cannot be attributed to In diffusion because In diffusion should shrink the effective thickness of the topological layer and increase the size of the gap. The smaller gap must therefore be due to superlattice dispersion. Because the gap in the heterostructure is no larger than the gap in the single thin film, it is clear that there is no In diffusion from the topmost trivial layer into the topmost topological layer and the heterostructure consists of sharp interfaces.

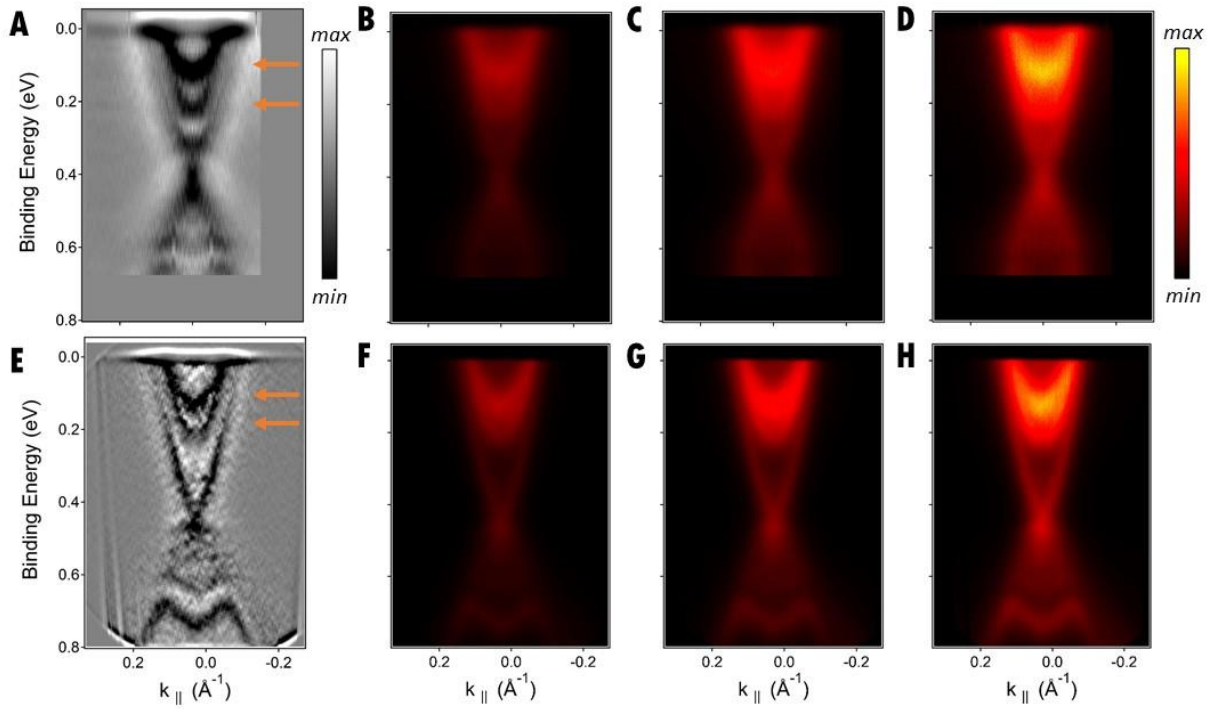


**fig. S5. Bulk quantum well states of 4QL/2QL 15% and 4QL/1QL 20%.** (A) A second-derivative map of the ARPES spectrum of 4QL/2QL 15%, shown in Fig. 2G of the main text. We clearly see two quantum well states in the bulk conduction band, marked by the orange arrows. (B–D) The same cut, with different color scales, to make the two quantum well states visible in the raw data. (E) The same as main text Fig. 3B, repeated here for completeness. Again, we clearly see two quantum well states in the bulk conduction band. (F–H) The same cut, with different color scales, to make the two quantum well states visible in the raw data.